East European Journal of Physics. 2. 436–444 (2026)
DOI: 10.26565/2312-4334-2026-2-49 ISSN 2312-4334

ELECTROMAGNETIC PROPERTIES OF A HYBRID SOLID-STATE STRUCTURE INCORPORATING A PLASMA-LIKE MEDIUM AND A METASURFACE

N.N. Beletskii, O.Yu. Averkov, Yu.O. Averkov*
O. Ya. Usikov Institute for Radiophysics and Electronics of the National Academy of Sciences of Ukraine, 12, Acad. Proskura Str., Kharkiv, 61085, Ukraine
**Corresponding Author e-mail: yuriyaverkov@gmail.com*
Received February 24, 2026; revised April 5, 2026; accepted May 6, 2026

In this paper, we theoretically investigate the dispersion properties of surface and bulk-surface electromagnetic waves propagating in a hybrid layered solid-state structure containing an isotropic plasmonic metasurface. This structure consists of a semi-infinite dielectric 1, an isotropic metasurface, a dielectric layer 2, and a semi-infinite plasma-like medium. We derive an exact analytical dispersion relation for the coupled electromagnetic modes and perform a comprehensive numerical analysis of it. Our analysis demonstrates how the metasurface conductivity, the dielectric layer thickness, and the semiconductor plasma frequency significantly influence the resonant interaction of the surface waves. It has been revealed that adding a plasma-like medium as a substrate leads to the emergence of hybrid surface waves and the possibility of bulk-surface waves. In fact, we found a significant difference between metal and semiconductor substrates. Indeed, to obtain exactly the same splitting value in a system with a metal substrate, a dielectric spacer approximately seven times thicker is required. This geometry difference makes semiconductors a much more practical choice for deep subwavelength miniaturization. The results provide a theoretical basis for the development and optimization of novel tunable waveguides, sensors, and slow-wave devices operating in the microwave and terahertz frequency ranges.

Keywords: *Plasmonic metasurface; Dielectric layer; Semiconductor; Plasma-like medium; Surface electromagnetic wave; Bulk-surface electromagnetic wave; Dispersion relation*

PACS: 78.67.Pt, 73.20.Mf, 72.30.+q

1. INTRODUCTION

Nanophotonics and optoelectronics today depend heavily on finding new ways to manipulate electromagnetic waves at the subwavelength level. In this context, two-dimensional metamaterials, or metasurfaces, have become the subject of intense research interest because they exhibit electrodynamic properties that simply do not exist in natural media [1]. Plasmonic metasurfaces are of particular interest. Such structures are powerful tools for light control, enabling tight field confinement, individual routing of surface waves, and precise control of photon density states. Fundamental theory of

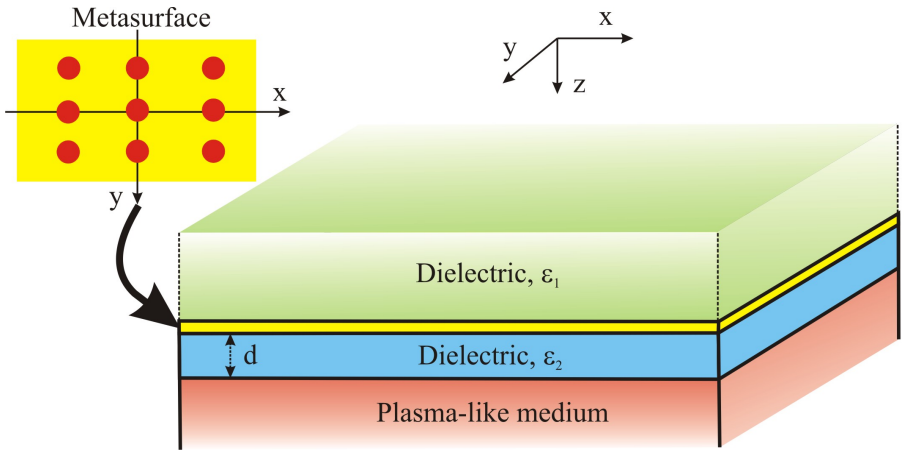

Figure 1. Geometry of the structure.

plasmonic metasurfaces has already clarified many of their unusual dispersion characteristics. For example, previous studies have shown that these metasurfaces support highly localized hybrid electromagnetic waves. Their spectrum is usually divided into two separate branches associated with hybrid transverse electric (TE) and transverse magnetic (TM) modes [2, 3]. A distinctive feature of these systems is that their isofrequency contours can transform from closed elliptical shapes to open hyperbolas as the frequency changes—a phenomenon known as an optical topological transition [4]. To

Cite as: N.N. Beletskii, O.Yu. Averkov, Yu.O. Averkov, East Eur. J. Phys. 2, 436 (2026), https://doi.org/10.26565/2312-4334-2026-2-49

accurately model these effects, it is necessary to carefully determine the effective surface conductivity, a parameter that can be successfully extracted using a combination of far-field and near-field measurements [5].

Applying anisotropic metasurface concepts to natural two-dimensional materials such as black phosphorus or graphene, as well as to complex multilayer heterostructures, provides even greater flexibility for wave control. Doped 2D materials naturally support strongly directional hyperbolic plasmons, and their routing can be dynamically tuned using an electric gate [6]. Interestingly, strong field localization can also occur at the physically tilted edges of these anisotropic sheets [7]. When multiple metasurfaces are stacked on top of each other, the interactions of their eigenmodes become quite complex. Some studies even draw a parallel between these coupled optical states and Feynman paths in electron transport [8]. From a theoretical point of view, the analysis of such stratified systems is most conveniently and rigorously performed using the transfer matrix formalism [9].

Recent work has considerably broadened the known classes of guided modes and dispersion regimes supported by engineered metasurfaces. In particular, analytical models for metasurfaces with anisotropic polarizabilities and arbitrary incident angles have been developed [10], engineered equifrequency contours have been used to realize self-collimated surface-wave steering [11], and twisted anisotropic heterometasurfaces have been shown to support hybrid surface waves [12]. In parallel, hyperbolic shear metasurfaces [13] and antihyperbolic surface waves on hyperbolic metasurfaces [14] have revealed additional possibilities for tailoring axial dispersion, confinement, and modal topology in artificial anisotropic platforms.

Recent studies have also demonstrated the possibility of realizing a scattering-free plasmonic Brewster effect via isotropic metasurfaces, including the all-angle regime for p-polarized surface waves [15].

Due to their strong anisotropy and tunability, these structures enable a wide range of specialized electromagnetic effects. Recent publications highlight their use to achieve nearly perfect spin selectivity of photons [16] and highly sensitive chiral probing [17]. They also serve as an excellent means for generating quantum photon-plasmon states under nonlinear conditions [18]. Because surface plasmons are so strongly confined near these structures, they can exert enormous transverse optical forces on neighboring nanoparticles [19] or contribute to highly directional radiative heat transfer [20]. Other practical applications include multi-band polarization converters [21] and fast helicity switches, often implemented using reversible Babinet checkerboard patterns [22, 23] or periodic arrangements of polariton cylinders [24].

Despite rapid developments in this field, some complex hybrid configurations still lack a detailed electrodynamic description. One such system is an asymmetric solid-state structure in which a dielectric layer is located between a plasmonic metasurface and a semi-infinite plasma-like medium (e.g., a semiconductor or metal). In this article, we theoretically and numerically investigate the dispersion characteristics of electromagnetic waves propagating through this geometry. Our main goal is to establish the exact conditions that lead to strong localization of electromagnetic waves and to investigate the frequency splitting effect of coupled surface modes guided at different interfaces of the solid-state structure with an isotropic plasmonic metasurface.

2. PROBLEM STATEMENT

2.1. Main equations and boundary conditions

Consider a flat-layered solid-state structure consisting of a semi-infinite dielectric with dielectric permittivity ε_1, a plasmonic metasurface, a dielectric layer with thickness d and dielectric permittivity ε_2, bordering on a semi-infinite plasma-like solid medium (a semiconductor or metal, see Fig. 1). The axis Oz is perpendicular to the boundary between the media and points deep into the plasma-like medium. The plane $z = 0$ coincides with the plane of the metasurface. The physical implementation of a metasurface is a periodic array of conductive thin discs, whose thickness, like the period, is much smaller than the wavelength. In this case, the electrodynamic response of such a structure can be described by macroscopic isotropic effective surface conductivity σ without taking into account spatial dispersion normal to the interface. The expression for σ will be given below. Electromagnetic fields in the structure under consideration are described by Maxwell's equations:

$$\nabla \times \mathbf{H}(\mathbf{r}, t) = \frac{1}{c}\frac{\partial \mathbf{D}(\mathbf{r}, t)}{\partial t} + \frac{4\pi}{c}\mathbf{j}(\mathbf{r}, t), \tag{1}$$

$$\nabla \times \mathbf{E}(\mathbf{r}, t) = -\frac{1}{c}\frac{\partial \mathbf{B}(\mathbf{r}, t)}{\partial t}, \tag{2}$$

$$\nabla \cdot \mathbf{D}(\mathbf{r}, t) = 0, \tag{3}$$

$$\nabla \cdot \mathbf{B}(\mathbf{r}, t) = 0. \tag{4}$$

where e is the electron charge, $\mathbf{E}(\mathbf{r}, t)$ is the electric field vector, $\mathbf{B}(\mathbf{r}, t)$ is the magnetic induction vector, and $\mathbf{H}(\mathbf{r}, t)$ is the magnetic field vector; for all media considered below, $\mu = 1$, hence, in Gaussian units, $\mathbf{B}(\mathbf{r}, t) = \mathbf{H}(\mathbf{r}, t)$. Here $\mathbf{D}(\mathbf{r}, t)$ is the electric displacement vector, $\mathbf{j}(\mathbf{r}, t) = (\mathbf{j}_\tau(\mathbf{r}, t), 0)$ and $\mathbf{j}_\tau(\mathbf{r}, t) = \mathbf{j}_\tau(\boldsymbol{\rho}, t)\delta(z)$ is the surface current in the metasurface plane, $\boldsymbol{\rho} = (x, y, 0)$ is the radius-vector in the $z = 0$-plane, $\delta(z)$ is the Dirac delta function.

Let us represent electromagnetic fields using Fourier integrals of the following form [25]:

$$\mathbf{E}(\mathbf{r},t) = \int\limits_{-\infty}^{\infty}\int\limits_{-\infty}^{\infty} \mathbf{E}(\boldsymbol{k},\omega)\exp\left[i(k_z z + \boldsymbol{\kappa}\boldsymbol{\rho} - \omega t)\right] d\boldsymbol{k}\, d\omega, \tag{5}$$

where ω denotes the angular frequency, $\boldsymbol{k} = (\boldsymbol{\kappa}, k_z)$ is the wave vector, $\boldsymbol{\kappa} = (k_x, k_y, 0)$ is the wave vector in the $z = 0$-plane, k_z is the normal component of the wave vector.

The material equations linking the electric displacement vector to the electric field intensity vector are described, in general, by the following non-local relationship:

$$D_j(\mathbf{r},t) = \int_{-\infty}^{t} \hat{\varepsilon}_{jg}(t-t')E_g(\mathbf{r},t')dt', \tag{6}$$

where indices j and g take values x, y, z, and summation is performed over index g. The kernel $\hat{\varepsilon}_{jg}(t-t')$ represents the dielectric response tensor of the medium. The dependence of the type $t - t'$ means the homogeneity of the structure's electrodynamic properties over time. For the Fourier components of fields, this material ratio takes the form:

$$D_j(\boldsymbol{k},\omega) = \varepsilon_{jg}(\omega)E_g(\boldsymbol{k},\omega). \tag{7}$$

Here, $\varepsilon_{jg}(\omega)$ is the frequency-dependent dielectric permittivity tensor, defined as the Fourier transform of the temporal response function $\hat{\varepsilon}_{jg}(\tau)$:

$$\varepsilon_{jg}(\omega) = \int_0^{\infty} \hat{\varepsilon}_{jg}(\tau)\exp(i\omega\tau)d\tau. \tag{8}$$

In the dielectric regions ($z < 0$ and $0 < z < d$), we have $\hat{\varepsilon}_{ij}(\tau) = \varepsilon_d\delta_{ij}\delta(\tau)$, where δ_{ij} is the Kronecker delta symbol. Then the constitutive relation (7) takes the form $\mathbf{D}_{1,2}(\boldsymbol{k},\omega) = \varepsilon_{1,2}\mathbf{E}(\boldsymbol{k},\omega)$. For plasma-like region ($z > d$) we have $\mathbf{D}_p(\boldsymbol{k},\omega) = \varepsilon_p(\omega)\mathbf{E}(\boldsymbol{k},\omega)$, where

$$\varepsilon_p(\omega) = \varepsilon_0 - \frac{\omega_p^2}{\omega(\omega + i\nu)}, \tag{9}$$

ε_0 is the high-frequency permittivity, ω_p is the plasma frequency of charge carriers in the plasma-like medium, and ν is the effective collision frequency accounting for dissipative losses.

We represent the surface current $\mathbf{j}_\tau(\boldsymbol{\rho},t)\delta(z)$ as

$$\mathbf{j}_\tau(\boldsymbol{\rho},t) = \int\limits_{-\infty}^{\infty}\int\limits_{-\infty}^{\infty} \mathbf{j}_\tau(\boldsymbol{\kappa},\omega)\exp\big[i(\boldsymbol{\kappa}\boldsymbol{\rho} - \omega t)\big] d\boldsymbol{\kappa} d\omega, \tag{10}$$

where

$$\mathbf{j}_\tau(\boldsymbol{\kappa},\omega) = \sigma(\omega)\, E(\boldsymbol{\kappa},\omega), \tag{11}$$

$\sigma(\omega)$ is the Fourier transform of the effective conductivity of a metasurface,

$$\sigma(\omega) = \frac{c}{4\pi}\left(\sigma_\infty + \frac{iA\omega}{\omega^2 - \Omega^2 + i\gamma\omega}\right), \tag{12}$$

where σ_∞ is the background conductivity accounting for the lower electronic bands contributions ($\mathrm{Re}\sigma_\infty = 0$), A is defined by the metasurface design ($\mathrm{Im}A = 0$), Ω is the metasurface resonant frequency, γ is the bandwidth of the resonance, defined by ohmic and radiation losses. In the future, we will not take into account dissipative losses in the metasurface as well as in plasma-like medium and will assume $\gamma = 0$ and $\nu = 0$.

The boundary conditions in the metasurface plane $z = 0$ are the conditions of continuity of the tangential components of the electric field intensity vectors and the jumps of the tangential components of the magnetic field intensity vectors associated with the presence of surface current:

$$\mathbf{n}_{1,2} \times \Big(\mathbf{E}_2(\boldsymbol{r},t) - \mathbf{E}_1(\boldsymbol{r},t)\Big) = 0, \tag{13}$$

$$\mathbf{n}_{1,2} \times \Big(\mathbf{H}_2(\boldsymbol{r},t) - \mathbf{H}_1(\boldsymbol{r},t)\Big) = \frac{4\pi}{c}\boldsymbol{j}_\tau(\boldsymbol{\rho},\boldsymbol{t}), \tag{14}$$

where $\mathbf{n}_{1,2} = (0,0,1)$ is a unit normal vector pointing from medium 1 to medium 2. The boundary conditions at the interface between dielectric 2 and the plasma-like medium ($z = d$) are the continuity conditions of the tangential components of the electric and magnetic fields:

$$\mathbf{n}_{1,2} \times \Big(\mathbf{E}_2(\boldsymbol{r},t) - \mathbf{E}_1(\boldsymbol{r},t)\Big) = 0,\ \mathbf{n}_{1,2} \times \Big(\mathbf{H}_2(\boldsymbol{r},t) - \mathbf{H}_1(\boldsymbol{r},t)\Big) = 0. \tag{15}$$

2.2. Dispersion relations of structure eigenwaves

Let us obtain the dispersion relation for p-polarized eigenwaves of the structure under study with field components $\mathbf{E}(\boldsymbol{r},t) = (E_x(\boldsymbol{r},t), 0, E_z(\boldsymbol{r},t))$, $\mathbf{H}(\boldsymbol{r},t) = (0, H_y(\boldsymbol{r},t), 0)$ and assume that waves propagate along the x-axis, i.e. $\boldsymbol{k} = (k_x, 0, k_z)$. For the selected polarization, the boundary conditions (13)-(15) take the form:

$$E_{x2}(x,t)\Big|_{z=0} = E_{x1}(x,t)\Big|_{z=0}, \tag{16}$$

$$H_{y2}(x,t)\Big|_{z=0} - H_{y1}(x,t)\Big)\Big|_{z=0} = -\frac{4\pi}{c} j_x(\boldsymbol{\rho},t)\Big|_{z=0}, \tag{17}$$

$$E_{x2}(x,t)\Big|_{z=d} = E_{x1}(x,t)\Big|_{z=d},\ H_{y2}(x,t)\Big|_{z=d} = H_{y1}(x,t)\Big)\Big|_{z=d}. \tag{18}$$

First, we obtain the dispersion relation for the *surface waves* of the structure under investigation. Hereafter, we will use the following dimensionless variables and structure parameters:

$$\xi = \frac{\omega}{\Omega},\ q = \frac{ck_x}{\Omega},\ \eta_{1,2} = i\frac{ck_{z1,2}}{\Omega} = \sqrt{q^2 - \xi^2\varepsilon_{1,2}},\ \eta_p = i\frac{ck_{zp}}{\Omega} = \sqrt{q^2 - \xi^2\varepsilon_p(\xi)} \tag{19}$$

$$\bar{A} = \frac{A}{\Omega},\ \bar{\omega}_p = \frac{\omega_p}{\Omega},\ \bar{\sigma}_\infty = -\frac{4\pi i}{c}\sigma_\infty,\ \delta = \frac{d\Omega}{c}. \tag{20}$$

Expressions (9) and (12) for the Fourier transforms of dielectric permittivity of the plasma-like medium and conductivity in dimensionless forms are written as follows:

$$\varepsilon_p(\xi) = \varepsilon_0 - \frac{\bar{\omega}_p^2}{\xi^2},\ \bar{\sigma}(\xi) = -\frac{4\pi i}{c}\sigma(\omega) = \bar{\sigma}_\infty + \frac{\bar{A}\xi}{\xi^2 - 1}. \tag{21}$$

Using the representation of fields (5) and surface current (10) from boundary conditions (16)-(18), we obtain the following dispersion relation for the surface eigenwaves:

$$\left[\xi\left(\frac{\varepsilon_1}{\eta_1} + \frac{\varepsilon_2}{\eta_2}\right) - \bar{\sigma}(\xi)\right]\left(\frac{\varepsilon_p(\xi)}{\eta_p} + \frac{\varepsilon_2}{\eta_2}\right) - \left[\xi\left(\frac{\varepsilon_1}{\eta_1} - \frac{\varepsilon_2}{\eta_2}\right) - \bar{\sigma}(\xi)\right]\left(\frac{\varepsilon_p(\xi)}{\eta_p} - \frac{\varepsilon_2}{\eta_2}\right)\exp(-2\eta_2\delta) = 0. \tag{22}$$

In the limit $\delta \to \infty$, the dispersion relation (22) decouples into two independent relations describing the eigenwaves of the isolated subsystems: dielectric 2 / plasma-like medium and dielectric 1 / metasurface / dielectric 2:

$$\xi\left(\frac{\varepsilon_1}{\eta_1} + \frac{\varepsilon_2}{\eta_2}\right) - \bar{\sigma}(\xi) = 0. \tag{23}$$

Let us consider *bulk-surface* eigenwaves whose fields decrease exponentially in dielectric 1 and plasma-like medium, but have an oscillatory character in dielectric 2. For these waves, the condition $\xi^2\varepsilon_1 < q^2 < \xi^2\varepsilon_2$ is satisfied. We introduce the following notation for the normal component of the wave vector in dielectric 2:

$$\zeta_2 = \frac{ck_{z2}}{\Omega} = \sqrt{\xi^2\varepsilon_2 - q^2}. \tag{24}$$

Satisfying the boundary conditions (16)-(18), we obtain the desired dispersion relation:

$$\left[\zeta_2^2\frac{\varepsilon_p(\xi)}{\eta_p}\left(\xi\frac{\varepsilon_1}{\eta_1} - \bar{\sigma}(\xi)\right) - \xi\varepsilon_2^2\right]\tan(\zeta_2\delta) - \varepsilon_2\zeta_2\left[\xi\left(\frac{\varepsilon_1}{\eta_1} + \frac{\varepsilon_p(\xi)}{\eta_p}\right) - \bar{\sigma}(\xi)\right] = 0. \tag{25}$$

Below, we will perform a numerical analysis of dispersion relations (22) and (25).

3. NUMERICAL ANALYSIS OF DISPERSION RELATIONS

For the numerical calculation of dispersion curves, we will select the following structure parameters: $\varepsilon_1 = 1$ (vacuum), $\varepsilon_2 = 2.1$ (teflon dielectric), $\varepsilon_0 = 15.68$ (InSb semiconductor) or $\varepsilon_0 = 1$ (metal), $\bar{\sigma}_\infty = 0.2$, $\bar{A} = 0.2$. We will only change the dimensionless quantities $\bar{\omega}_p$ and δ. Let us first consider the eigenspectrum of surface electromagnetic waves in the structure dielectric 1 - metasurface - dielectric 2, shown in Fig. 2. We see that only surface waves are present in the spectrum. Indeed, as follows from dispersion relation (23), for purely imaginary values of η_1 or η_2 (in the absence of dissipative losses), there are no real solutions to this relation. It can also be seen that the low-frequency branch ($\xi < 1$) of the spectrum (curve 4) originates at the beginning of the coordinates, while the high-frequency branch ($\xi > 1$, curve 5)

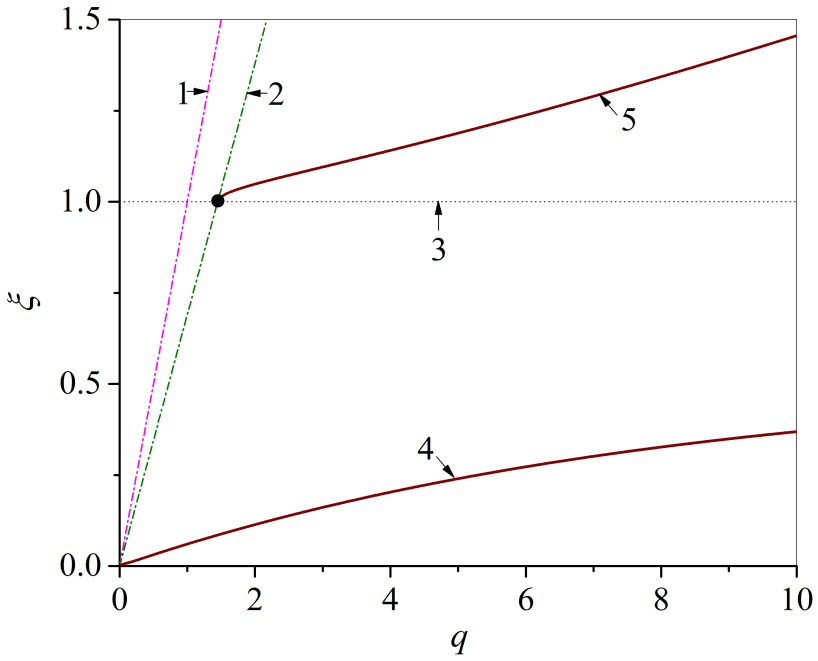

Figure 2. Eigenspectrum of surface electromagnetic waves in the structure dielectric 1 - metasurface - dielectric 2, calculated for the above-mentioned parameter values. Curves 1 and 2 correspond to the light lines in dielectrics 1 and 2, respectively. Curve 3 is for the dimensionless metasurface resonant frequency $\xi = 1$, curves 4 and 5 are for the low- and high frequency modes, respectively. The black circle corresponds to the starting point of the dispersion curve spectrum 5.

has its starting point on the light line 2. Note also that the low-frequency branch appears in the spectrum only when $\bar{\sigma}_\infty > 0$.

In Fig. 3 - Fig. 6, we analyze the effect of hybridization of surface eigenwaves in the structure dielectric 1 - metasurface - dielectric 2 - plasma-like medium, arising from the interaction of the high-frequency intrinsic surface wave of the "metasurface" with the eigenwave of the plasma-like medium as a substrate. We consider the influence of such structural parameters as the high-frequency dielectric permittivity of the plasma-like medium, its plasma frequency, and the thickness of the dielectric layer 2 on this effect. Fig. 3 shows the intrinsic spectrum of such a structure for a semiconductor substrate for $\bar{\omega}_p = 5$ and $\delta = 0.45$. Fig. 3 shows that taking into account the plasma-like medium leads to the appearance of an additional branch of the spectrum (curve 6), which, with an increase in the longitudinal wave number q, asymptotically tends towards the surface plasmon frequency ξ_{sp} and has a spectrum starting point at the light line 2. The region of interaction between the high-frequency mode of the metasurface (curve 7) and the mode of the plasma-like medium (curve 6) is also visible – region A, where dispersion curves 6 and 7 are closest to each other. The frequency gap in region A is $\Delta\xi \approx 0.0521$. Unlike the spectrum shown in Fig. 2, the presence of a plasma-like substrate leads to the appearance of so-called bulk-surface (or waveguide) modes, shown in Fig. 3 by dotted lines. The dispersion curves of these modes are located in the region between light lines 1 and 2 and transition into the dispersion curves of the corresponding surface modes. The amplitudes of the fields of the bulk-surface modes under consideration oscillate in the region of dielectric 2 and decrease monotonically along the normal in the regions of dielectric 1 and the plasma-like medium as they move deeper into these media. The bulk-surface mode corresponding to the high-frequency branch 7 has a spectrum starting point on the light line 1. Taking into account dissipative losses in the structure to the left of this point, there is a section of the dispersion curve corresponding to the so-called leaky mode [26]. Note that the region of greatest interaction (resonant interaction) of surface modes corresponding to dispersion curves 6 and 7 (region A) is located near the surface plasmon frequency ξ_{sp}, where the following relations hold: $\varepsilon_p(\xi) < 0$ and $\bar{\sigma}(\xi) > 0$.

Fig. 4 demonstrates the influence of the plasma frequency value on the position and magnitude of the frequency gap in the region of maximum interaction of surface modes. The dispersion curves in Fig. 4 are calculated for the same structure and with the same parameters as in Fig. 3, except for the plasma frequency value, $\bar{\omega}_p = 5.3$. Comparing Fig. 3 and Fig. 4 reveals that increasing the plasma frequency $\bar{\omega}_p$ at a fixed dielectric thickness δ shifts the resonant interaction zone (region A) toward higher frequencies and larger longitudinal wavenumbers q. Concurrently, the magnitude of the frequency splitting narrows down to $\Delta\xi \approx 0.0333$.

The influence of the thickness of the dielectric layer 2 on the structure of the dispersion curves 6 and 7 in the structure under consideration with a semiconductor substrate is shown in Fig. 5. The dispersion curves in Fig. 5 were constructed using the same structure parameters as in Fig. 3, except for the thickness of the dielectric 2, $\delta = 0.6$. As evident from comparing Figs. 3 and 5, expanding the dielectric layer thickness δ under a constant plasma frequency $\bar{\omega}_p$ reduces the frequency splitting to $\Delta\xi \approx 0.0171$. Numerical calculations confirm that the resonant interaction zone shifts toward

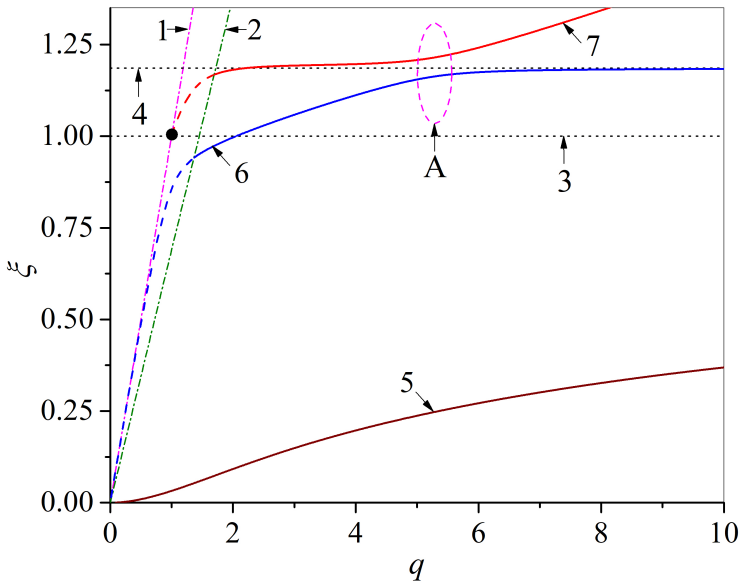

Figure 3. Eigenspectrum of the surface waves of the structure dielectric 1 - metasurface - dielectric 2 - InSb semiconductor, calculated for the above-mentioned dielectric and metasurface parameters and $\bar{\omega}_p = 5, \delta = 0.45$. Curves 1 and 2 correspond to the light lines in dielectrics 1 and 2, respectively. Curve 3 is for the dimensionless metasurface resonant frequency $\xi = 1$, curve 4 is for surface plasmon frequency $\xi_{sp} = \bar{\omega}_p/\sqrt{\varepsilon_0 + \varepsilon_2} \approx 1.2$, curve 5 is for the low frequency mode, curve 6 and 7 are hybridized high-frequency modes. The solid sections of curves 6 and 7 correspond to surface modes, while the dashed sections correspond to bulk-surface modes. Area A shows the area of resonant interaction between modes 6 and 7. The black circle corresponds to the starting point of the dispersion curve of bulk-surface mode.

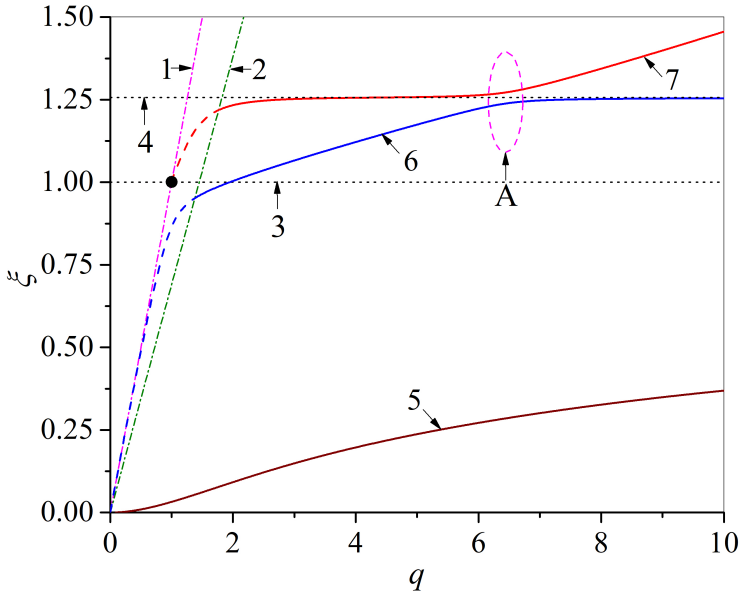

Figure 4. Eigenspectrum of the surface waves of the structure dielectric 1 - metasurface - dielectric 2 - InSb semiconductor, calculated for the above-mentioned dielectric and metasurface parameters and $\bar{\omega}_p = 5.3, \delta = 0.45$. Curves 1 and 2 correspond to the light lines in dielectrics 1 and 2, respectively. Curve 3 is for the dimensionless metasurface resonant frequency $\xi = 1$, curve 4 is for surface plasmon frequency $\xi_{sp} \approx 1.26$, curve 5 is for the low frequency mode, curve 6 and 7 are hybridized high-frequency modes. The solid sections of curves 6 and 7 correspond to surface modes, while the dashed sections correspond to bulk-surface modes. Area A shows the area of resonant interaction between modes 6 and 7. The black circle corresponds to the starting point of the dispersion curve of bulk-surface mode.

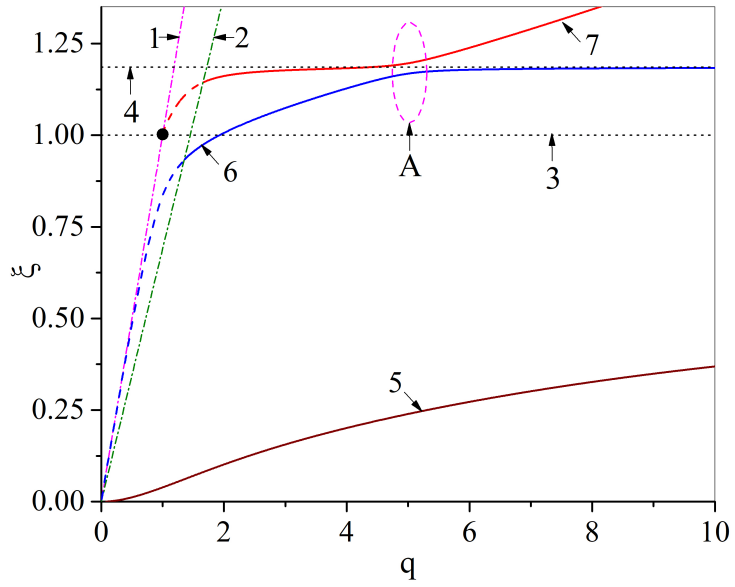

Figure 5. Eigenspectrum of the surface waves of the structure dielectric 1 - metasurface - dielectric 2 - InSb semiconductor, calculated for the above-mentioned dielectric and metasurface parameters and $\bar{\omega}_p = 5$, $\delta = 0.6$. Curves 1 and 2 correspond to the light lines in dielectrics 1 and 2, respectively. Curve 3 is for the dimensionless metasurface resonant frequency $\xi = 1$, curve 4 is for surface plasmon frequency $\xi_{sp} \approx 1.2$, curve 5 is for the low frequency mode, curve 6 and 7 are hybridized high-frequency modes. The solid sections of curves 6 and 7 correspond to surface modes, while the dashed sections correspond to bulk-surface modes. Area A shows the area of resonant interaction between modes 6 and 7. The black circle corresponds to the starting point of the dispersion curve of bulk-surface mode.

smaller q values in this geometry.

Dispersion curves for the structure under investigation, where metal is selected as the plasma-like medium, are shown in Fig. 6. Comparing the semiconductor and metallic substrates (Figs. 3 and 6) demonstrates a striking contrast. For the same plasma frequency $\bar{\omega}_p$ and comparable mode splitting ($\Delta\xi \approx 0.052$), the high-frequency mode interaction in the metal-backed structure occurs at notably smaller wave vectors q. Achieving this exact splitting in the metallic case requires a dielectric spacer approximately seven times thicker than its semiconductor counterpart. It should also be noted that for all structures considered in the field of resonant interaction, the conditions $\varepsilon_p(\xi) < 0$ and $\bar{\sigma}(\xi) > 0$ are satisfied.

4. DISCUSSION AND CONCLUSION

We have developed a rigorous electrodynamic model to study the dispersion features of localized electromagnetic waves in a hybrid solid-state structure, combining a plasmonic metasurface with a plasma-like substrate. We obtained an analytical expression for the eigenmodes of the studied structure, which are coupled modes of the metasurface and the plasma-like medium. The numerical analysis shows that the presence of a plasma-like medium significantly changes the spectrum of electromagnetic waves compared to isolated metasurfaces. In particular, it allows bulk-surface waves to propagate and causes strong hybridization between the eigenmodes of metasurface and surface plasmons of the substrate.

The degree of this mode coupling is highly sensitive to the geometry and material properties. Our calculations show that the frequency splitting $\Delta\xi$ (the gap between the interacting branches) is governed primarily by the dimensionless dielectric spacer thickness δ. It has been demonstrated that widening this gap weakens the field overlap, predictably narrowing the splitting. Furthermore, tuning the plasma frequency $\bar{\omega}_p$ of the substrate allows one to shift the resonant interaction zone across the frequency-wave vector plane. In practice, this could be achieved through optical pumping, thermal heating, or electrical gating of the semiconductor. We also determined the frequency and wave vector range in which bulk-surface waves transition into leaky waves, which is an important factor in estimating radiation losses in practical devices. A comparison of the semiconductor (InSb) and metal substrates shows the profound influence of dielectric contrast.

We found that to achieve a similar degree of mode separation in a structure with a metal substrate, a dielectric layer approximately seven times thicker than that required for a semiconductor is needed. This significant geometric difference highlights the clear advantage of using semiconductor substrates for applications focused on deep miniaturization with sub-wavelength dimensions. Ultimately, the ability to selectively control the phase velocity, field localization, and spectral gaps of these hybrid waves provides a robust physical foundation for creating advanced microwave and terahertz components, from compact delay lines and sensors to dynamic cloaking coatings.

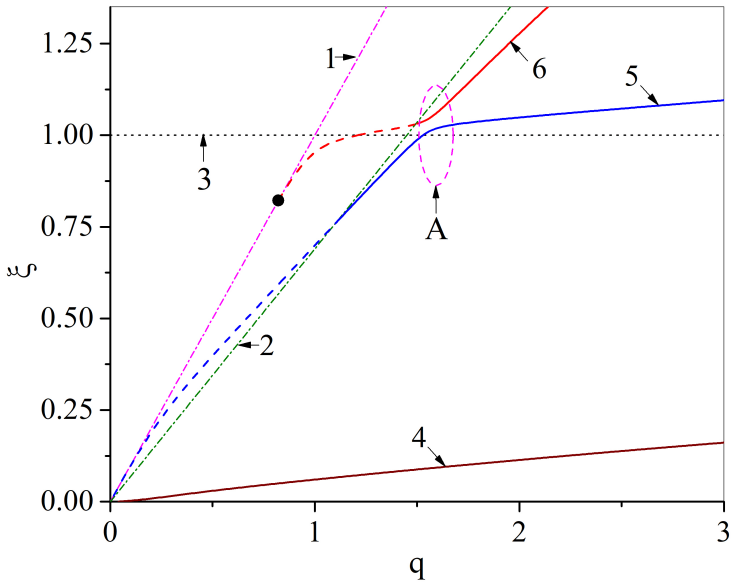

Figure 6. Eigenspectrum of the surface waves of the structure dielectric 1 - metasurface - dielectric 2 - metal, calculated for the above-mentioned dielectric and metasurface parameters and $\bar{\omega}_p = 5$, $\delta = 3.3$. Curves 1 and 2 correspond to the light lines in dielectrics 1 and 2, respectively. Curve 3 is for the dimensionless metasurface resonant frequency $\xi = 1$, curve 4 is for the low frequency mode, curve 5 and 6 are hybridized high-frequency modes. The solid sections of curves 5 and 6 correspond to surface modes, while the dashed sections correspond to bulk-surface modes. Area A shows the area of resonant interaction between modes 5 and 6. The black circle corresponds to the starting point of the dispersion curve of bulk-surface mode.

ORCID

N.N. Beletskii, https://orcid.org/0000-0002-3194-7251; **O.Yu. Averkov**, https://orcid.org/0000-0002-1169-9393; **Yu.O. Averkov**, https://orcid.org/0000-0001-6055-015X

REFERENCES

[1] A. Ranjbar and A. Grbic, "Broadband, Multiband, and Multifunctional All-Dielectric Metasurfaces," Phys. Rev. Applied, **11**, 054066 (2019). https://doi.org/10.1103/PhysRevApplied.11.054066

[2] D. Correas-Serrano, J. S. Gomez-Diaz, A. Alvarez-Melcon, and A. Alù, "Black phosphorus plasmonics: anisotropic elliptical propagation and nonlocality-induced canalization," J. Opt., 18, 104006 (2016). https://doi.org/10.1088/2040-8978/18/10/104006

[3] J. S. Gomez-Diaz, M. Tymchenko, and A. Alù, "Hyperbolic Plasmons and Topological Transitions Over Uniaxial Metasurfaces," Phys. Rev. Lett., 114, 233901 (2015). https://doi.org/10.1103/PhysRevLett.114.233901

[4] A. A. High, R. C. Devlin, A. Dibos, M. Polking, D. S. Wild, J. Perczel, N. P. de Leon, M. D. Lukin, and H. Park, "Visible-frequency hyperbolic metasurface," Nature, **522**, 192–196 (2015). https://doi.org/10.1038/nature14477

[5] C. L. Holloway, E. F. Kuester, J. A. Gordon, J. O'Hara, J. Booth, and D. R. Smith, "An overview of the theory and applications of metasurfaces: The two-dimensional equivalents of metamaterials," IEEE Antennas Propag. Mag., **54**, 10–35 (2012). https://doi.org/10.1109/MAP.2012.6230714

[6] A. Nemilentsau, T. Low, and G. Hanson, "Anisotropic 2D Materials for Tunable Hyperbolic Plasmonics," Phys. Rev. Lett., **116**, 066804 (2016). https://doi.org/10.1103/PhysRevLett.116.066804

[7] P. A. D. Gonçalves, L. P. Bertelsen, S. Xiao, and N. A. Mortensen, "Hybridized Plasmons in 2D Nanoslits: From Graphene to Anisotropic 2D Materials," ACS Photonics, 4, 2645–2652 (2017). https://doi.org/10.1021/acsphotonics.7b00558

[8] J. Sperrhake, M. Falkner, S. Fasold, T. Kaiser, and T. Pertsch, "Equivalence of reflection paths of light and Feynman paths in stacked metasurfaces," Phys. Rev. B, **102**, 245108 (2020). https://doi.org/10.1103/PhysRevB.102.245108

[9] T. Zhan, X. Shi, Y. Dai, X. Liu, and J. Zi, "Transfer matrix method for optics in graphene layers," J. Phys.: Condens. Matter, **25**, 215301 (2013). https://doi.org/10.1088/0953-8984/25/21/215301

[10] I. Allayarov, V. R. Tuz, A. Cala Lesina, and A. B. Evlyukhin, "Analytical model of metasurfaces comprising meta-atoms with anisotropic polarizabilities and for arbitrary incident angles," Phys. Rev. B, **111**, 155438 (2025). https://doi.org/10.1103/PhysRevB.111.155438

[11] S. M. Kandil, D. J. Bisharat, and D. F. Sievenpiper, "Engineering equifrequency contours of metasurfaces for self-collimated surface-wave steering," Phys. Rev. Applied, **21**, 044006 (2024). https://doi.org/10.1103/PhysRevApplied.21.044006

[12] X. Zhang, C. Bian, Z. Gong, R. Chen, T. Low, H. Chen, and X. Lin, "Hybrid surface waves in twisted anisotropic heterometasurfaces," Phys. Rev. Applied, **21**, 064034 (2024). https://doi.org/10.1103/PhysRevApplied.21.064034

[13] E. M. Renzi, E. Galiffi, X. Ni, and A. Alù, "Hyperbolic Shear Metasurfaces," Phys. Rev. Lett., 132, 263803 (2024). https://doi.org/10.1103/PhysRevLett.132.263803

[14] C. Bian, X. Zhang, W. Ma, X. Chen, H. Chen, T. Low, and X. Lin, "Antihyperbolic surface waves on hyperbolic metasurfaces," Phys. Rev. A, **111**, 033522 (2025). https://doi.org/10.1103/PhysRevA.111.033522

[15] X. Zhang, X. Cui, T. Cai, W. Cai, T. Low, H. Chen, and X. Lin, "Scattering-free Plasmonic Brewster Effect via Metasurfaces," ACS Photonics, **12**(4), 1865–1872 (2025). https://doi.org/10.1021/acsphotonics.4c02263

[16] R. Ogier, Y. Fang, M. Käll, and M. Svedendahl, "Near-Complete Photon Spin Selectivity in a Metasurface of Anisotropic Plasmonic Antennas," Phys. Rev. X, **5**, 041019 (2015). https://doi.org/10.1103/PhysRevX.5.041019

[17] S. Droulias and L. Bougas, "Chiral sensing with achiral anisotropic metasurfaces," Phys. Rev. B, **104**, 075412 (2021). https://doi.org/10.1103/PhysRevB.104.075412

[18] C. L. Cortes, W. Newman, S. Molesky, and Z. Jacob, "Quantum nanophotonics using hyperbolic metamaterials," J. Opt., **14**, 063001 (2012). https://doi.org/10.1088/2040-8978/14/6/063001

[19] N. K. Paul, D. Correas-Serrano, and J. S. Gomez-Diaz, "Giant lateral optical forces on Rayleigh particles near hyperbolic and extremely anisotropic metasurfaces," Phys. Rev. B, 99, 121408(R) (2019). https://doi.org/10.1103/PhysRevB.99.121408

[20] Y. Zhang, M. Antezza, H.-L. Yi, and H.-P. Tan, "Metasurface-mediated anisotropic radiative heat transfer between nanoparticles," Phys. Rev. B, **100**, 085426 (2019). https://doi.org/10.1103/PhysRevB.100.085426

[21] B.-Q. Lin, J.-X. Guo, P. Chu, W.-J. Huo, Z. Xing, B.-G. Huang, and L. Wu, "Multiple-Band Linear-Polarization Conversion and Circular Polarization in Reflection Mode Using a Symmetric Anisotropic Metasurface," Phys. Rev. Applied, **9**, 024038 (2018). https://doi.org/10.1103/PhysRevApplied.9.024038

[22] Y. Nakata, Y. Urade, K. Okimura, T. Nakanishi, F. Miyamaru, M.W. Takeda, and M. Kitano, "Anisotropic Babinet-Invertible Metasurfaces to Realize Transmission-Reflection Switching for Orthogonal Polarizations of Light," Phys. Rev. Applied, **6**, 044022 (2016). https://doi.org/10.1103/PhysRevApplied.6.044022

[23] Y. Nakata, K. Fukawa, T. Nakanishi, Y. Urade, K. Okimura, and F. Miyamaru, "Reconfigurable Terahertz Quarter-Wave Plate for Helicity Switching Based on Babinet Inversion of an Anisotropic Checkerboard Metasurface," Phys. Rev. Applied, **11**, 044008 (2019). https://doi.org/10.1103/PhysRevApplied.11.044008

[24] C.P. Mavidis, A.C. Tasolamprou, E.N. Economou, C.M. Soukoulis, and M. Kafesaki, "Polaritonic cylinders as multifunctional metamaterials: Single scattering and effective medium description," Phys. Rev. B, **102**, 155310 (2020). https://doi.org/10.1103/PhysRevB.102.155310

[25] J. D. Jackson, *Classical Electrodynamics*, 3rd ed. (John Wiley & Sons, New York, 1999).

[26] R.S. Brazis, "Active and nonlinear interactions under excitation of plasma-type polaritons in semiconductors," Litov. Fiz. Sb., **21**(4), 73-117 (1981). (in Russian)

ЕЛЕКТРОМАГНІТНІ ВЛАСТИВОСТІ ГІБРИДНОЇ ТВЕРДОТІЛЬНОЇ СТРУКТУРИ, ЩО ВКЛЮЧАЄ ПЛАЗМОПОДІБНЕ СЕРЕДОВИЩЕ ТА МЕТАПОВЕРХНЮ

М.М. Білецький, **О.Ю. Аверков**, **Ю.О. Аверков**

Інститут радіофізики та електроніки ім. О. Я. Усикова НАН України, вул. Акад. Проскури, 12, Харків, 61085, Україна

У цій статті ми теоретично досліджуємо дисперсійні властивості поверхневих і об'ємно-поверхневих електромагнітних хвиль, що поширюються в гібридній шаруватій твердотільній структурі, яка містить ізотропну плазмонну метаповерхню. Ця структура складається з напівнескінченного діелектрика 1, ізотропної метаповерхні, діелектричного шару 2 і напівнескінченного плазмоподібного середовища (напівпровідника або металу). Ми виводимо точне аналітичне дисперсійне співвідношення для зв'язаних електромагнітних мод і проводимо його детальний чисельний аналіз. Наш аналіз демонструє, що провідність метаповерхні, товщина діелектричного шару та плазмова частота напівпровідника значно впливають на резонансну взаємодію поверхневих хвиль. Було виявлено, що додавання плазмоподібного середовища як підкладки призводить до появи гібридних поверхневих хвиль та можливості виникнення об'ємно-поверхневих хвиль. Фактично, ми виявили значну різницю між металевими та напівпровідниковими підкладками. Дійсно, щоб отримати точно таке саме значення розщеплення в системі з металевою підкладкою, необхідний діелектричний прошарок, товщина якого приблизно в сім разів більша. Ця геометрична різниця робить напівпровідники набагато більш практичним вибором для глибокої субхвильової мініатюризації. Результати надають теоретичну основу для розробки та оптимізації нових перебудовних хвилеводів, датчиків та пристроїв на повільних хвилях, що працюють у діапазонах мікрохвильових та терагерцових частот.

Ключові слова: *плазмонна метаповерхня; діелектричний шар; напівпровідник; плазмоподібне середовище; поверхнева електромагнітна хвиля; об'ємно-поверхнева електромагнітна хвиля; дисперсійне співвідношення*